

## Structural morphology and electronic properties of the Si-Cr interface

A. Franciosi, D. J. Peterman, and J. H. Weaver

*Synchrotron Radiation Center, University of Wisconsin-Madison,  
Stoughton, Wisconsin 53589*

V. L. Moruzzi

*IBM T. J. Watson Research Center, Yorktown Heights, New York 10598*

(Received 16 November 1981)

Photoemission studies ( $12 \leq h\nu \leq 135$  eV) of room-temperature formation of the Si-Cr interface show reactive behavior with atomic intermixing and dramatic modifications of the metal-derived  $d$  density of states. Self-consistent augmented-spherical-wave calculations of the total and  $l$ -projected densities of states for the silicides  $\text{Cr}_3\text{Si}$ ,  $\text{CrSi}$ , and  $\text{CrSi}_3$  in simplified cubic lattice structures allow an identification of general trends in the electronic structure upon Si-Cr heteropolar bond formation. These experimental and theoretical results suggest an interface morphology where a Si-rich intermixed phase is present for a depth of  $\approx 10$  monolayers between the Si crystal and the unreacted Cr film. Evidence of Si segregation in the top layers of the Cr film is provided.

### I. INTRODUCTION

Silicon-metal junctions have a well-known importance in modern electronics technology and a large number of experimental and theoretical efforts have been devoted to defining the basic mechanisms which determine their electronic and structural properties.<sup>1-6</sup> These diverse efforts are revealing fascinating physical and chemical properties of interfaces, properties which have important ramifications in the fundamental understanding of interfacial phenomena and in the technological use of semiconductor devices.<sup>7,8</sup>

Si-refractory metal interfaces are extremely interesting systems in connection with very large scale integrated-circuit technology,<sup>8</sup> but their microscopic structural and electronic properties have received very little attention. In this paper we deal with the mechanisms driving Si-Cr interface formation.

We have conducted valence-band and core-level photoemission studies with synchrotron radiation as a function of metal deposition on the Si(111)-(2×1) surface. We have also performed calculations of the electronic structure for a series of Si-Cr model compounds to gain insight into the modification of the electronic states due to Si-Cr heteropolar bond formation.

Among the important conclusions of the present

study are the following.

(1) The intrinsic Si surface-state emission is dramatically reduced at submonolayer Cr coverage but there is no detectable change of the Fermi-level pinning position.

(2) At room temperature, an intermixed phase of metallic character is formed at the silicon-chromium interface and comparison of experimental and theoretical results suggests that this intermixed phase is Si-rich.

(3) The valence-band emission and measured Schottky barrier height of this interface differ from what is expected for a Si-CrSi<sub>2</sub> interface.

The implication is that the Si-Cr interface may not follow trends observed for other Si-metal interfaces. In other reactive interfaces, the intermixed phases formed at room temperature have electronic structures similar to those of the "bulk" silicides grown by high-temperature film reaction.<sup>1,4,5</sup> In Si-Cr, the intermixed phase is metallic whereas the bulk silicide CrSi<sub>2</sub> is expected to be a small-gap semiconductor. Si-refractory metal interfaces show, in fact, remarkably different properties for compound growth (stoichiometry and kinetics)<sup>8,9</sup> from other Si-metal interfaces. For the Si-near-noble-metal interfaces, for example, moderate annealing (250°C) results in growth of Ni<sub>2</sub>Si, Pd<sub>2</sub>Si,

and Pt<sub>2</sub>Si with a square-root-of-time growth kinetics, while for the silicon—refractory-metal interfaces only disilicides grow on a macroscopic scale (upon annealing<sup>8,9</sup> at  $\approx 600^\circ\text{C}$ ) with a linear time dependence.

This paper represents a continuation of a study of the electronic properties of silicides and silicon-metal interfaces. In a previous paper<sup>10</sup> we discussed photoemission measurements of bulk VSi<sub>2</sub>, MoSi<sub>2</sub>, and TaSi<sub>2</sub> and compared them to calculated densities of states for V-Si and Mo-Si compounds. We are now extending those studies to CrSi<sub>2</sub> and emphasizing the interface,<sup>10,11</sup> hoping that experimental investigations of interface and bulk properties and parallel theoretical studies will lead to a better understanding of these important systems.

## II. EXPERIMENTAL AND THEORETICAL TECHNIQUES

Room-temperature Si-Cr interfaces were prepared *in situ* in an ultrahigh vacuum photoelectron spectroscopy system (operating pressure  $\sim 3 \times 10^{-11}$  Torr). *N*-type, phosphorous-doped (1.5  $\Omega$  cm) Si single crystals oriented along the [111] direction were cut to give posts  $4 \times 4 \times 10$  mm<sup>3</sup>. These were mounted onto copper sample holders, loaded onto a bank (capacity  $\sim 20$ ), and retrieved immediately before measurements were undertaken. Clean Si(111)-(2 $\times$ 1) surfaces were prepared by cleaving at precut notches in the side of the Si post. Samples were then positioned at the common focus of the monochromatic radiation beam and the electron energy analyzer. Surface cleanliness was monitored by detecting the Si(111) intrinsic surface states and by Auger spectroscopy. A detailed discussion of the geometry of the system can be found in Ref. 12.

Interfaces were prepared by Cr sublimation from a Ta boat at pressures always better than  $2 \times 10^{-10}$  Torr during deposition, with recovery to the operating pressure ( $\sim 3 \times 10^{-11}$  Torr) within  $\sim 1$  min after deposition.<sup>13</sup> The metal coverage of the Si substrate,  $\Theta$ , was monitored with a quartz thickness monitor and throughout this paper is given in terms of the Si(111) surface atomic density ( $\Theta = 1$  monolayer at  $7.6 \times 10^{14}$  atoms/cm<sup>2</sup>). Studies of the interface were carried out for metal coverages of 0.1 to 50 monolayers<sup>11</sup>; the data presented here represent numerous cleaves and repetitive measurements of the various stages of interface formation.

Synchrotron radiation from the 240-MeV elec-

tron storage ring Tantalus at the University of Wisconsin, Madison, was monochromatized with a 3-m toroidal grating monochromator (photon energy range 12–135 eV) and a Seya-Namioka monochromator ( $12 \leq h\nu \leq 30$  eV). The emitted photoelectrons were energy analyzed with a commercial double-pass cylindrical mirror analyzer with a typical overall resolution (electrons plus photons) of 0.3–0.4 eV.

The energy band calculations for Si-Cr compounds were based on the augmented-spherical-wave (ASW) procedure for the solution of the one-electron equations.<sup>14,15</sup> Exchange and correlation effects were treated in the local-density approximation. Self-consistency was pursued until the calculated electronic charges were unchanged to within 0.001 electrons within the Wigner-Seitz sphere. The calculations were parameter-free, the atomic number and the crystal structure being the only *a priori* inputs used, and correspond to theoretical equilibrium since the atomic spacing was systematically varied until the total energy was minimized.

## III. EXPERIMENTAL RESULTS

Metal coverages of  $0.1 \leq \Theta \leq 50$  monolayers were obtained on Si substrates kept at room temperature. Systematic studies of the photoelectron energy distribution curves (EDC's) as a function of chromium deposition were performed at several photon energies. The main Si-derived features of the valence-band emission and the intrinsic surface state emission were monitored at  $h\nu = 12$  eV. The Cr-derived *3d* contribution to the valence-band emission dominated at 21 eV. Valence-band results were also obtained at higher photon energies ( $30 \leq h\nu \leq 120$  eV), but, due to the very slight  $h\nu$  dependence of the spectral features, these results are not reported here. The Si *2p* core was studied at  $h\nu = 120$  and 135 eV, photon energies which allowed a variation in the surface sensitivity of the measurements through the change of the photoelectron escape depth and thereby made it possible to obtain information about the depth dependence of interface composition.

The effects of Cr deposition onto clean Si(111)-(2 $\times$ 1) are shown in Fig. 1 through EDC's at  $h\nu = 12$  eV. The bottommost EDC of Fig. 1 shows the well-known Si valence band features for clean Si(111),<sup>16</sup> including the surface-state feature at  $0.73 \pm 0.1$  eV below  $E_F$ . Successive EDC's displaced upward correspond to increasing Cr cover-

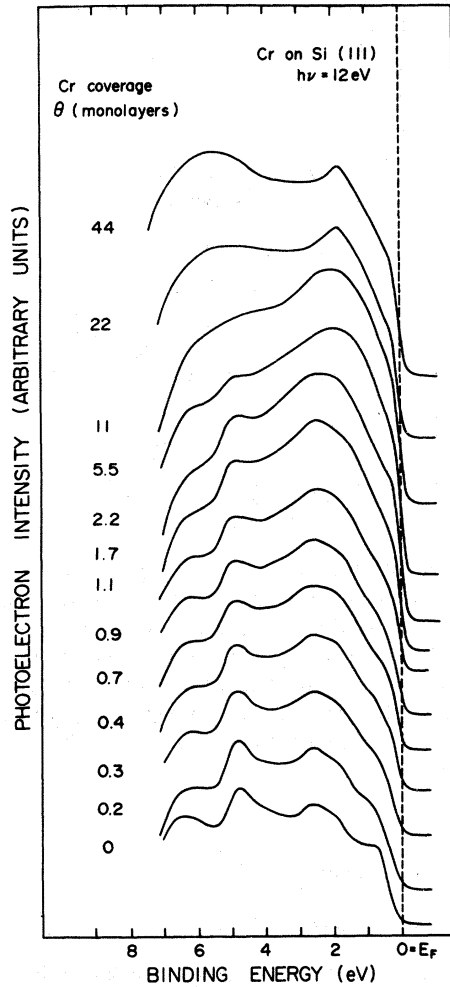


FIG. 1. Representative photoelectron energy distribution curves (EDC's) for  $h\nu = 12$  eV showing changes of the valence-band emission during formation of the Si-Cr interface. Bottommost EDC is for clean Si(111)-(2 $\times$ 1). At high coverages ( $\Theta \geq 20$ ) the valence-band emission is indistinguishable from that of bulk Cr (Ref. 17). For  $1-2 \lesssim \Theta \lesssim 9-10$  the EDC's show the formation of intermixed Si-Cr species of metallic character.

age. The upper EDC's of Fig. 1 ( $\Theta > 22$ ) reveal the bulk Cr valence-band emission. The emission spectra of Fig. 1 were reproducible within the experimental uncertainty for coverages obtained with a single evaporation or with a series of submonolayer depositions.

At the lowest metal coverages ( $0 < \Theta \leq 0.3$ ), the Si(111) intrinsic surface-state emission is sharply reduced but no variation of the Fermi-level pinning position can be detected (within 0.1 eV) as seen, for example, from the binding energy of the Si valence-band feature at  $4.8 \pm 0.1$  eV from  $E_F$ . Fur-

ther metal deposition ( $0.3 \lesssim \Theta \lesssim 1$ ) gives rise to a gradual increase of the emission intensity at  $E_F$ . At this stage of interface formation, only very slight modifications of the Si bulk valence-band features are seen at  $h\nu = 12$  eV. At metal coverages  $\Theta \geq 1.1-1.7$ , a well-defined Fermi edge is visible and the Si valence-band features (2.70 and 1.88 eV from  $E_F$ ) are now dominated by a broad Cr-derived structure at  $-2.35$  eV. This structure shifts toward  $E_F$  with coverage while increasing in intensity with respect to the other spectral features. For  $\Theta \geq 20$  monolayers, the valence-band emission is indistinguishable from that of bulk Cr.<sup>17</sup>

In Fig. 2 we show EDC's for  $h\nu = 21$  eV for which the Cr-derived 3d character is more visible than at lower photon energy. Again, the bottommost EDC shows the well-known<sup>16</sup> clean Si(111) valence-band and surface-state emission features. Figure 2 shows that for  $\Theta \geq 1$  the valence band is dominated by Cr-derived 3d emission but that for coverages  $\Theta < 11$  the valence band is dramatically different from that of bulk Cr. For comparison we have plotted (uppermost EDC) the valence-band spectrum obtained for a thick ( $\sim 300$  Å) Cr film evaporated onto oxidized tantalum.<sup>17</sup> Comparison shows that the main 3d peak of bulk Cr (labeled A) appears to be shifted toward lower binding energy and the structure (labeled B) centered 3 eV below  $E_F$  is absent for  $\Theta \leq 12$ . Peak A exhibits an interesting coverage dependence: For  $1 \leq \Theta \leq 10$  it shifts with coverage toward  $E_F$ , then for metal coverages  $\Theta > 10$  it shifts back toward its final position 1.2 eV below  $E_F$ , while feature B increases dramatically in intensity. In the inset of Fig. 2 the position of peak A is plotted versus metal coverage.

It is evident from Figs. 1 and 2 that the interface EDC's for  $\Theta \leq 10-12$  cannot be obtained from a superposition of contributions from Si(111) and bulk Cr. Figure 2 suggests that there are several coverage intervals that correspond to different behaviors in the valence-band emission. This is confirmed by measurements of the integrated intensity and the binding energy of the Si 2p levels as a function of metal coverage at a photon energy of 120 eV for which the surface sensitivity for the Si 2p emission<sup>18</sup> is about the same as for the valence-band results at  $h\nu = 21$  eV. In Fig. 3 the Si 2p binding energy is plotted as a function of metal coverage together with representative EDC's for  $\Theta = 0$  and 11. Very little variation is seen for  $\Theta \leq 1-2$  and  $\Theta \geq 9-10$  but for  $1-2 \lesssim \Theta \lesssim 9-10$  the formation of an extended interface (see Discussion) corresponds to a Si 2p core energy shift of

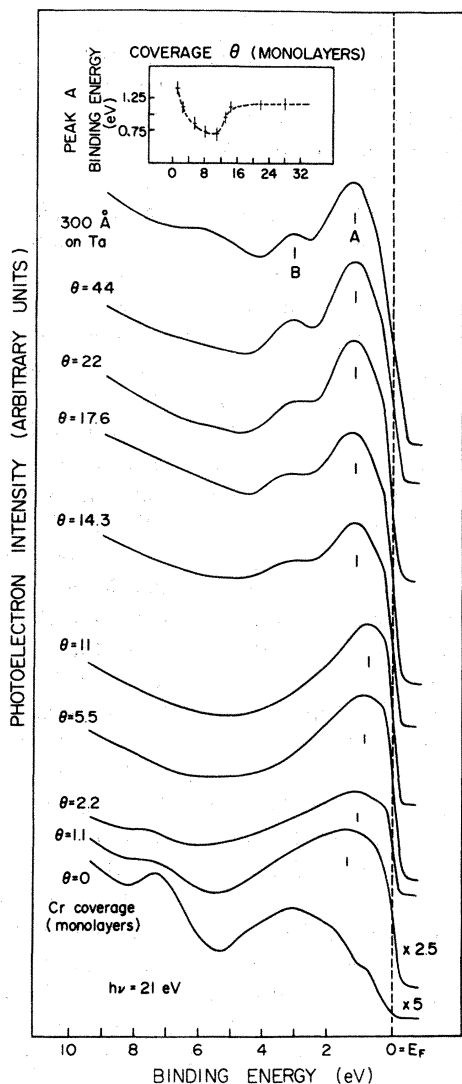


FIG. 2. Representative EDC's for  $h\nu=21$  eV showing the effect of increasing Cr coverage. The uppermost EDC is representative of a thick Cr film ( $\sim 300$  Å) deposited on oxidized Ta. The valence-band spectra from the intermixed Si-Cr species ( $\Theta \approx 10$ ) show a shift of the main  $3d$  peak (labeled A) towards lower binding energy with respect to bulk Cr and the absence of the deeper  $3d$  structure B, in agreement with what is expected for the formation of Si-rich silicidelike phases. In the inset the position of peak A is plotted vs metal coverage. For  $\Theta > 10$  the shift is readily explained by the presence of an increasing amount of unreacted metal. For  $\Theta < 10$  local bonding distortions in the intermixed region rather than a stoichiometry gradient may explain the observed behavior

$0.20 \pm 0.1$  eV toward lower binding energy.

The Si  $2p$  integrated intensity for a given coverage,  $I_{2p}(\Theta)$ , normalized to the Si substrate emission,  $I_{2p}(0)$ , can be used to define an attenuation

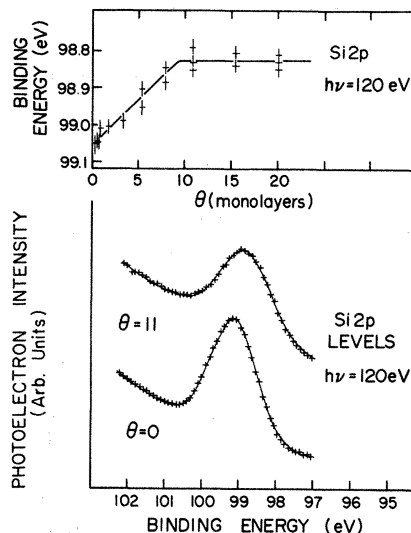


FIG. 3. Binding energy of the Si  $2p_{3/2}$  level as a function of metal coverage  $\Theta$ . Representative EDC's for the clean Si(111)- $(2 \times 1)$  surface and  $\Theta=11$  are also shown. For  $1-2 \lesssim \Theta \lesssim 9-10$  the formation of an intermixed region corresponds to a shift of  $0.2 \pm 0.1$  eV of the Si  $2p$  levels toward higher binding energy, while very little variation is seen for  $\Theta \lesssim 1-2$  and  $\Theta \gtrsim 10$ .

coefficient  $\alpha$  where

$$\alpha = \ln[I_{2p}(\Theta)/I_{2p}(0)] .$$

With such a definition a sharp interface with no atomic intermixing will show a linear dependence of  $\alpha$  with coverage, the slope being determined by the escape depth (see the Appendix). The values of  $\alpha$  measured at  $h\nu=120$  eV during room-temperature formation of the Si-Cr interface are plotted in Fig. 4 as a function of coverage (solid line). Also shown (dashed lines) are selected values of  $\alpha$  obtained with  $h\nu=135$  eV for which the surface sensitivity is greater. For comparison we show (dot-dashed line) the attenuation coefficient, calculated assuming no atomic intermixing and an escape depth  $L$  of  $10$  Å.<sup>18</sup> Comparison shows that for  $\Theta \lesssim 8-9$  the attenuation rate of the Si  $2p$  emission is less than expected for a sharp, nonreactive interface. For  $9-10 \lesssim \Theta \lesssim 20$  the experimental behavior is approximately linear with a slope in quantitative agreement with the theoretical one. For  $\Theta > 20$  it departs from linearity and tends to a rather constant value. Again, these results suggest three different coverage ranges: the low coverage interval ( $\Theta \lesssim 1-2$ ), the intermediate interval ( $1-2 \lesssim \Theta \lesssim 10$ ), and the high coverage interval

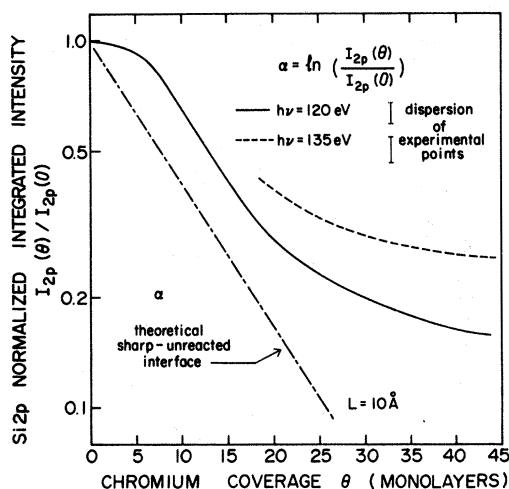


FIG. 4. Log-linear plot of the attenuation coefficient  $\alpha$  of the Si  $2p$  emission  $I_{2p}$  vs metal coverage. Solid line:  $h\nu = 120$  eV (escape depth 10–12 Å). Dashed line:  $h\nu = 135$  eV (escape depth 5–7 Å). Dot-dashed line: Ideal attenuation coefficient for a sharp unreacted interface (Frank–van der Merwe-type film growth) with escape depth  $L = 10$  Å. The experimental lines are the best fit of about 50 data points for each curve, at coverages  $\Theta = 0.1-1, 2, 5, 11, 17, 22, 33, 44$ . The average dispersion of the experimental points is given by the error bars in the upper right corner. For  $1-2 \lesssim \Theta \lesssim 8-9$  the formation of intermixed species corresponds to an attenuation rate slower than expected for a sharp unreacted interface. For  $10 \leq \Theta \leq 20$  the data reflect an escape-depth-driven exponential attenuation of the interface emission. For  $\Theta \geq 20$  emission from silicon atoms segregated at the Cr-vacuum interface explains the experimental behavior.

( $\Theta > 10$ ). It will be convenient to discuss each of these intervals separately in the Discussion section.

#### IV. CALCULATIONS

In order to study the stoichiometry dependence of the electronic structure of Si-Cr compounds, self-consistent energy-band calculations were performed for three stoichiometries:  $\text{Cr}_3\text{Si}$ ,  $\text{CrSi}$ , and  $\text{CrSi}_3$ .<sup>19</sup> To isolate the stoichiometry dependence as much as possible, the atoms were taken to occupy the sites of an fcc lattice for all three stoichiometries. That is, the three-to-one compounds were taken to have the  $\text{Cu}_3\text{Au}$  structure and  $\text{CrSi}$  was taken to have the  $\text{CuAu}$  structure. While these structures are simpler than those observed (they are close packed with 12 nearest neighbors), they appear to adequately describe the

stoichiometry dependence of the chemical bonding as reflected by the site and angular-momentum resolved state densities.<sup>20</sup> For example, the behavior of the  $p$ - $d$  states as a function of the metal content and the estimates of charge transfer, as derived from similar model calculations<sup>21</sup> and from semiempirical calculations using realistic silicide structures,<sup>22</sup> were found to be in remarkable agreement for Pd silicides.

The present calculations show that for Cr silicides the metal- $d$ –silicon- $p$  coupling is the dominant aspect of the chemical bonding and that the modifications of the density of states within 3 eV of  $E_F$  (most relevant for the interpretation of our photoemission spectra) upon Si-Cr bond formation can be understood in terms of a decrease of metal-metal hybridization due to the reduction of the Cr-Cr interaction as Si content is increased.

To emphasize the modifications of the valence-band states for different silicide stoichiometries, we show in Fig. 5 the total density of states for Cr (Ref. 23),  $\text{Cr}_3\text{Si}$ ,  $\text{CrSi}$ , and  $\text{CrSi}_3$ ; we also show the  $l$ -decomposed densities of states (DOS) giving the Cr-derived  $d$  character (Fig. 6), the Si-derived  $p$  character (Fig. 6), and the Cr  $s$ - $p$  character compared to the Si-derived  $s$ - $d$  character (Fig. 7).<sup>24</sup> In what follows we analyze the prototypical results for  $\text{Cr}_3\text{Si}$  to characterize the different regions of the DOS and then turn to  $\text{CrSi}$  and  $\text{CrSi}_3$  for comparison.

The DOS results for  $\text{Cr}_3\text{Si}$  in Figs. 5–7 show an occupied  $d$ -bandwidth of  $\sim 6$  eV with sharp structures near  $-1.1$ ,  $-2.3$ , and  $-3.6$  eV. Three different energy regions can be distinguished in the DOS.

(1) Between  $-8$  and  $-12$  eV, a Si-derived  $s$  band is shown to have negligible coupling with metal  $d$  states. The band contains about 1.2 electrons per Si atom, accounting for most of the occupied Si  $s$  states. The small metal  $s$ - $p$  contribution visible in Fig. 7 accounts for a few percent of the calculated charge per Cr atom, and we therefore conclude that the Si  $3s$  states are not significantly involved in the bonding with the metal. Calculations for near-noble-metal silicides<sup>21,22</sup> show similar behavior.

(2) Between  $-3.0$  and  $-7$  eV, the total DOS for  $\text{Cr}_3\text{Si}$  has a main peak at about  $-3.6$  eV with other features between  $-4$  and  $-7$  eV. All structures arise from bonding combinations of Si- $p$  and Cr- $d$  states. A comparison with the density of states for pure Cr (topmost curve in Fig. 5) shows that in the silicide the  $p$ - $d$  bonding interaction splits and sub-

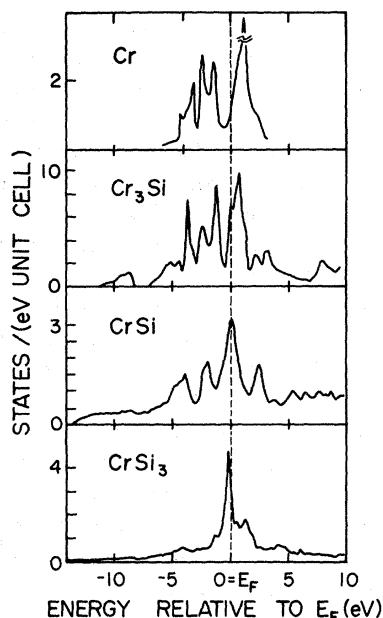


FIG. 5. Total density of states (DOS) for Cr (Ref. 23),  $\text{Cr}_3\text{Si}$  (calculated with  $\text{Cu}_3\text{Au}$  structure),  $\text{CrSi}$  ( $\text{CuAu}$ ), and  $\text{CrSi}_3$  ( $\text{Cu}_3\text{Au}$ ). While the  $\text{Cr}_3\text{Si}$  DOS shows similarities with the bulk Cr case, increasing Si content in the compound results in compression of the DOS around  $E_F$  due to the decrease of the  $d$ - $d$  hybridization. For  $\text{CrSi}_3$  one structure close to  $E_F$  (FWHM  $\sim 0.5$  eV) accounts for nearly 50% of the calculated  $d$  charge per Cr atom.

stantially lowers part of the metal  $d$  bands. Figure 7 shows that  $\sim 50\%$  of the calculated  $p$  charge per Cr atom contributes to a partial  $\text{Cr}-p$  DOS that reproduces the main features of the  $\text{Si}-p$  and  $\text{Cr}-d$  DOS between  $-3$  and  $-7$  eV. This suggests  $d$ - $p$  hybridization of the metal bonding orbitals.

(3) Between  $-3$  eV and  $E_F$  the metal  $d$  states account for all the features of the  $\text{Cr}_3\text{Si}$  total DOS with little contribution from Si-derived orbitals. This energy region contains the dominant structures of the spectrum and accounts for about 3.2  $d$  states per Cr atom.

The calculated charge transfer can be related to the ionicity of the Si-metal bonding.<sup>25</sup> For  $\text{Cr}_3\text{Si}$  we found 4.1 electrons on Si atoms corresponding to a very small charge transfer from the metal to the Si (0.03 electrons per metal atom). Analogously we estimated for  $\text{CrSi}$  and  $\text{CrSi}_3$  a charge transfer of 0.05 and 0.10 electrons per metal atom, respectively, from Cr to Si. These results suggest that the ionicity is of secondary importance in determining the silicide valence states but that a

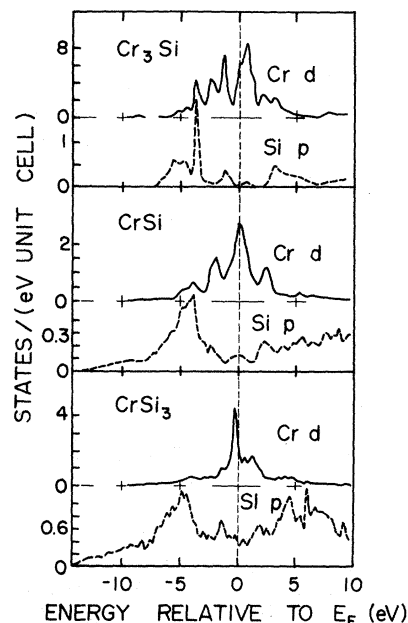


FIG. 6.  $I$  projection of the DOS for  $\text{Cr}_3\text{Si}$ ,  $\text{CrSi}$ , and  $\text{CrSi}_3$  in simplified cubic structures. The Cr  $d$  character is compared to the Si  $p$  character. For Cr silicides, as for the near-noble-metal ones, the metal- $d$ —silicon- $p$  coupling is the dominant aspect of the chemical bonding. Between  $-3.0$  and  $-7$  eV ( $\text{Cr}_3\text{Si}$ ) the bonding combination of metal  $d$  states and Si  $p$  states account for most of the DOS features. The states within  $-3$  eV from  $E_F$  reflect mainly Cr  $d$  character with little contribution from Si-derived orbitals.

small charge transfer from metal to silicon is expected.

A comparison of the DOS's for  $\text{CrSi}$  and  $\text{CrSi}_3$  with those for  $\text{Cr}_3\text{Si}$  allows the identification of several trends in the electronic structure.

(1) Because of increased Si-Si interaction the Si  $s$  bands broaden dramatically going from  $\text{Cr}_3\text{Si}$  to  $\text{CrSi}$  and  $\text{CrSi}_3$ . The gap that existed in  $\text{Cr}_3\text{Si}$  between the  $s$  band and the other valence states disappears in  $\text{CrSi}$  and  $\text{CrSi}_3$  so that  $s$  character is distributed on the energy scale up to  $E_F$ . Nevertheless, in all cases the deep-lying  $s$  states account for most of the  $s$  charge so that very little  $s$  contribution is seen within 6 eV of  $E_F$ . For all compounds, therefore, there is still very little coupling between the metal-derived states and the Si  $s$  states. It is the increasing Si-Si coordination that explains the broadening of occupied and empty  $s$  states.

(2) For  $\text{CrSi}$  the bonding combination of Cr  $d$  and Si  $p$  states largely accounts for the total DOS

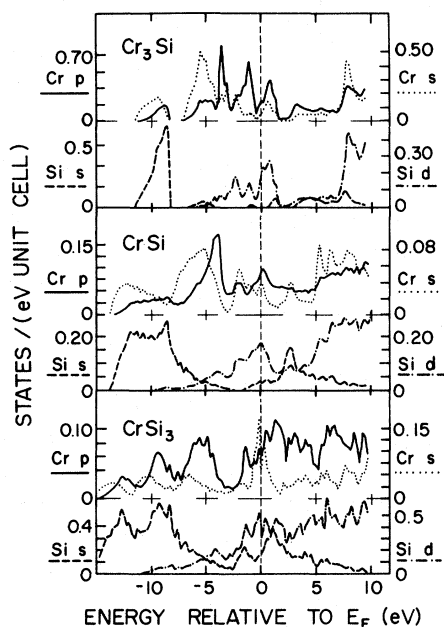


FIG. 7.  $l$  projection of the DOS for  $\text{Cr}_3\text{Si}$ ,  $\text{CrSi}$ , and  $\text{CrSi}_3$  in simplified cubic structures. The Cr  $s$  and  $p$  character is compared to the Si  $s$  and  $d$  character. The Si  $s$  states show negligible coupling with metal  $d$  states in all compounds. The Cr- $d$ —Si- $p$  hybridization is clearly the dominant aspect of the chemical bonding.

between  $-3$  and  $-6$  eV. The Si  $p$  partial DOS exhibits broadening with respect to  $\text{Cr}_3\text{Si}$  due to the increased Si-Si interaction. The structures below  $-6$  eV are related to Si-Si bonding states and are not influenced by the bonding with the metal. For  $\text{CrSi}_3$ , metal- $d$ —Si- $p$  bonding states extend on the energy scale between  $-2$  and  $-6$  eV because of the change of the metal  $d$  band width due to the decrease of the Cr-Cr interaction.

(3) The energy region between  $-3$  eV and  $E_F$ , which shows the most evident changes with stoichiometry, reflects mainly metal-derived  $d$  character and is the most important region for comparison with experimental spectra. The total DOS's in Fig. 5 show substantial compression of the  $d$  density of states toward  $E_F$  on going from  $\text{CrSi}$  to  $\text{CrSi}_3$ . For  $\text{CrSi}_3$  the  $d$  structure close to  $E_F$  [full width at half maximum (FWHM)  $\sim 0.5$  eV] accounts for nearly 50% of the calculated total  $d$  charge per Cr atom while all other structures between 3 eV and  $E_F$  lose intensity. Figures 6 and 7 show that the DOS in this region is mainly due to  $d$ - $d$  bonding and antibonding states, with very little contribution from Si-derived orbitals. The modifi-

cation of the DOS with increasing Si content can therefore be qualitatively understood in terms of a reduction of the  $d$ - $d$  hybridization due to the decrease of the Cr-Cr interaction in the Si-rich silicides.

## V. DISCUSSION

### A. Low coverage interval

In the very early stages of interface formation,  $0.1 \leq \Theta \leq 0.3$ , a drastic reduction of the Si intrinsic surface-state emission occurs without any apparent change of the Fermi-level pinning position (within 0.1 eV) or Si  $2p$  core-level binding energy. From the emission onset of the EDC's it is possible to measure the sample work function  $\Phi$  versus metal deposition. The value for the clean Si(111)-(2 $\times$ 1) surface was found to be  $4.65 \pm 0.10$  eV, in good agreement with the literature.<sup>26</sup> With increasing Cr deposition no work function variation was detected (within 0.1 eV) and for the thickest Cr films ( $\Theta > 50$ ) the measured value,  $\Phi = 4.60 \pm 0.10$  eV, corresponded to that of bulk Cr.<sup>27</sup>

The Schottky-barrier height  $\Phi_B$  at the interface is given by the value of the band bending for the clean  $n$ -Si(111) surface modified by the change in band bending induced by metal deposition. Since we detected no change in the Fermi-level pinning position as a function of metal coverage, the resulting Schottky-barrier height is the same as for clean Si where  $\Phi = E_C - E_F = 0.79 \pm 0.1$  eV.<sup>28</sup>

The removal of the intrinsic surface-state emission at submonolayer coverage seems a general aspect of Si-metal interfaces. Braicovich *et al.*<sup>2</sup> proposed that this phenomenon is related to the first stage of the chemical reaction which results in an extended, reacted interface. No fundamental difference should exist, then, in the chemical behavior at submonolayer coverage and subsequent stages of interface formation. However, our results suggest that the bonding of metal atoms with Si differs in these two regions. In particular for  $\Theta \leq 1-2$  no detectable change of the Si  $2p$  binding energy was observed (Fig. 3) while a small but definite shift was observed for  $1-2 \leq \Theta \leq 9-10$ . Furthermore, the attenuation rate of the Si  $2p$  is slower for  $\Theta \leq 1-2$  than for  $1-2 \leq \Theta \leq 9-10$ , with a definite change of slope in between (see the Appendix and Fig. 8). Studies of the Si-Au interface<sup>2</sup> also showed no shift of the Si  $2p$  and Au  $4f$  levels for  $\Theta \leq 2$  while the formation of an intermixed Si-Au phase was evidenced by a final shift of  $+0.4$  and  $-0.5$  eV of the Si  $2p$  and Au  $4f$ s,

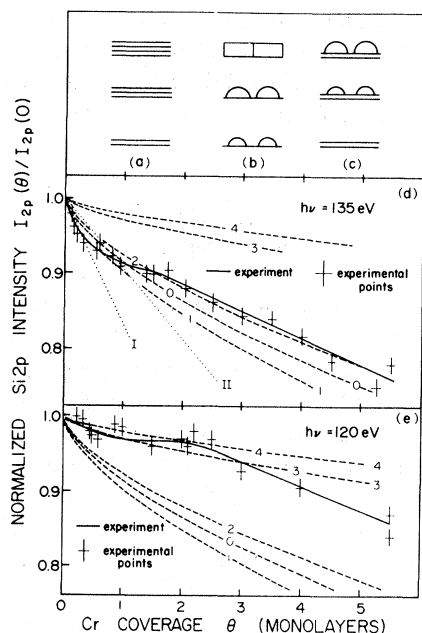


FIG. 8. Main growth mechanisms for an unreacted film (Ref. 35): (a) layer-by-layer or Frank-van der Merwe mode, (b) three-dimensional island growth or Volmer-Weber mode, (c) island growth on top of an intermediate continuous layer of thickness  $d$  or Stranski-Krastanov mode. We calculated the theoretical attenuation of the Si 2p emission for each mode assuming hemispherical islands of equal radii with an average island concentration of  $n_c$  islands/cm<sup>2</sup>. The parameters  $d$  and  $n_c$  are used to fit the experimental data. Comparison of theory and experiment for mode (a) can be found in Fig. 4 while modes (b) and (c) are compared here. (d) shows such a comparison for  $h\nu=135$  eV and (e) for  $h\nu=120$  eV. Dotted line: initial stage of Stranski-Krastanov growth mode (I:  $d=1$  Å,  $L=5$  Å; II:  $d=5$  Å,  $L=7$  Å). Dashed line: Volmer-Weber mode (0:  $n_c=1.17 \times 10^{12}$  isl/cm<sup>2</sup>, 1:  $n_c=1.74 \times 10^{12}$  isl/cm<sup>2</sup>, 2:  $n_c=7.94 \times 10^{11}$  isl/cm<sup>2</sup>, 3:  $n_c=4.10 \times 10^{10}$  isl/cm<sup>2</sup>, 4:  $n_c=1.50 \times 10^{10}$  isl/cm<sup>2</sup>; all with  $L=10$  Å). (d) shows that only a Volmer-Weber mode gives some agreement with experiment, but the same choice of parameters gives a theoretical curve that is in sharp disagreement with experiment for  $h\nu=120$  eV (e). The experimental behavior is therefore in quantitative disagreement with all three main mechanisms for nonreactive film growth.

respectively.

If interface formation at submonolayer metal coverage is to be interpreted solely as the first stage of a chemical reaction which results in an extended, reacted interface,<sup>2</sup> then the observed differences in core emission behavior for the two coverage ranges must be explained in terms of a different chemical environment of the metal atoms in

the two cases.<sup>29</sup> This has yet to be substantiated by analysis of the metal atom's chemical environment in the low coverage range.<sup>30</sup>

### B. The intermediate region ( $1-2 \lesssim \Theta \lesssim 9-10$ )

We have shown that for  $\Theta < 10-12$  monolayers the valence-band emission from the Cr-Si interface differs from that of bulk Cr (Fig. 2) because the width of the occupied  $d$  bands is reduced and their center is shifted toward the Fermi level. Clearly, the valence-band spectrum cannot be obtained by superimposing weighted contributions from Si(111) and bulk Cr. Instead, it is in good qualitative agreement with what is expected from our calculations for the formation of Si-rich silicidlike phases. Further, the attenuation rate of the Si 2p emission for  $1-2 \lesssim \Theta \lesssim 9-10$  is much slower than expected for a sharp, nonreactive interface (see Fig. 4 and the Appendix) and, in this coverage range, the cores shift  $0.2 \pm 0.1$  eV toward lower binding energy (Fig. 3). Again, such behavior is consistent with the results of our calculation. We therefore conclude that at the interface an intermixed region of  $\sim 10$  monolayers is formed, where Si-rich phases are present.

We will now examine in detail the experimental and theoretical evidence in favor of this interpretation. The photoemission spectra in Fig. 2 emphasize the metal derived  $d$  character due to the photon energy dependence of the Cr 3d cross section.<sup>17</sup> For  $\Theta \gtrsim 10$  the formation of the interface region is completed and the spectra increasingly resemble that of bulk Cr due to an increasing amount of unreacted metal. Compared to the photoemission spectra of bulk Cr, the spectra for  $\Theta \sim 10$  show that the  $d$  bands are shifted toward  $E_F$  and that the  $d$  derived structure at 3 eV is absent. This is consistent with a general trend observed in the model calculation for Cr-Si bond formation. As discussed above the DOS within 3 eV of  $E_F$  reflects metal-derived  $d$  character with minimal Si contribution; the replacement of Cr-Cr bonds with heteropolar Si-Cr bonds shifts the  $d$  character toward  $E_F$  with a decrease in overall width (reduced  $d-d$  hybridization). The calculations predict, for Si-rich Cr-Si phases, a trend toward a DOS dominated by a single structure within  $\sim 2$  eV of  $E_F$ , accounting for roughly half of the metal  $d$  charge, in qualitative agreement with the experiment for the intermixed phase.

The shift of the Si 2p core levels toward lower binding energy with increasing metal coverage

(completed for  $\Theta \sim 10$ ) has a direction and order of magnitude consistent with our expectation of a small but definite charge transfer from Cr to Si upon bond formation in intermixed Si-Cr species at the interface. Although the correlation between the core binding energy shift and charge transfer is not straightforward,<sup>25</sup> the observed behavior is consistent with what was found for Si-Ni interface formation where shifts of 0.4–0.6 eV toward lower binding energy were observed<sup>5</sup> and for which theory predicted<sup>22</sup> a small charge transfer from metal to Si atoms.

The slower attenuation of the Si 2*p* emission compared to that expected for a sharp, nonreactive interface can be understood in terms of an intermixed phase and is quantitatively inconsistent with three-dimensional island growth of an unreacted Cr film. The observed coverage dependence disagrees with the basic nonreactive growth mechanisms (see the Appendix for comparison with calculations of Volmer-Weber, Frank–van der Merwe, and Stranski-Krastanov growth mechanisms). Furthermore, in assuming three-dimensional island growth, one must explain the coverage dependence of the Si 2*p* binding energy and the disappearance (Fig. 2) of all bulk Si valence-band features for  $\Theta \sim 3$ . The bulk Si(111) feature at 7.5 eV is clearly visible for  $\Theta < 3$ , notwithstanding the higher Cr photoyield, and it is difficult to explain its behavior with coverage for island growth of a Cr film at  $\Theta \sim 3$ . The behavior of this Si feature can be explained by its extreme sensitivity to the breaking of tetrahedral coordination upon Si-metal reaction, as was shown in studies of the Si-Pd interface.<sup>31</sup>

In the inset of Fig. 2 we showed that for  $\Theta \leq 10$  peak *A* shifts toward  $E_F$  with increasing Cr coverage. Shifts of the center of mass of the occupied *d* levels with coverage have been observed during the formation of several silicon–near-noble-metal interfaces,<sup>1,4</sup> where Si-metal compounds have electronic structures close to those of bulk metal silicides.<sup>1,4</sup> The modifications of the valence band with metal coverages were usually attributed to a stoichiometry gradient in the intermixed phase with Si enrichment near the interface. Our band calculations for Si-Cr show that the direction of the observed shift is inconsistent with having a composition gradient normal to the interface; Si enrichment near the interface (Cr depletion) should result in a narrower *d* band shifted to lower binding energies. Instead, we suggest that the behavior of peak *A* reflects different chemical environments

and/or local bond distortions<sup>29</sup> in the intermixed region rather than a stoichiometry gradient. As recently pointed out by Ho *et al.*<sup>29</sup> in a very interesting paper, it is always very difficult to distinguish between the effect of true composition variations in the silicelike phase at the interface and the effect of local distortions of the Si–metal bonds.

### C. High coverage range and the Cr-vacuum interface ( $\Theta \geq 10$ )

Figure 2 shows that for  $\Theta \geq 10$  the valence-band emission tends gradually to that of bulk Cr, becoming indistinguishable from that of the metal at  $\Theta \sim 20$ . Si 2*p* core-level measurements show that for  $9 \leq \Theta \leq 20$  the 2*p* intensity decreases exponentially (Fig. 4), indicating that an unreacted Cr film “covers up” the intermixed interface.

At higher coverage ( $\Theta > 20$ ) our data give evidence of Si segregation in the upper few layers of the unreacted Cr film.<sup>11</sup> Figures 3 and 4 show that Si 2*p* emission is visible even at the highest coverages explored. Furthermore, for  $\Theta > 20$  the Si 2*p* attenuation (Fig. 4) departs from exponential behavior and the Si 2*p* emission approaches a nearly constant value of  $I_{2p}(\Theta)/I_{2p}(0) \simeq 0.10–0.15$  ( $h\nu = 120$  eV). A value  $\sim 1.7$  times larger is determined from the results at  $h\nu = 135$  eV where the surface sensitivity is greater (escape depth 5–7 Å), as shown by the dashed curve in Fig. 4 for which  $I_{2p}(\Theta)/I_{2p}(0) \simeq 0.20–0.25$ , providing evidence of Si enrichment in the topmost layer of the evaporated film. Data for the Si-Pd (Ref. 22), Si-V (Ref. 32), and Si-Cr (Ref. 10) interfaces after heat treatment all showed substantial Si segregation at the metal-vacuum interface. We showed that, to a smaller extent, this occurs even at room temperature for Si-Cr. It is possible to roughly estimate the amount of Si segregated on the metal film by calculating the thickness *d* of a Si “bulk crystal,” which will give rise to the same 2*p* core emission intensity observed at the highest metal coverage. Assuming

$$\frac{I_{2p}(\Theta)}{I_{2p}(0)} \Big|_{\Theta \rightarrow \infty} \simeq \frac{I_{2p}(\Theta)}{I_{2p}(0)} \Big|_{\Theta \rightarrow 50} \simeq \text{const}$$

it is

$$\frac{I_{2p}(\Theta)}{I_{2p}(0)} \Big|_{\Theta \rightarrow \infty} \simeq 1 - e^{-d/L},$$

where *L* is the photoelectron escape depth for bulk

Si. For both  $h\nu=120$  and  $135$  eV we obtain  $d \sim 1.5 \pm 0.5$  Å, i.e., the equivalent of 0.6–1.3 monolayers. Since the Si  $2p$  levels at high metal coverage have the same binding energy as for  $\Theta \sim 10$ , similar Si–Cr bonding may be present in the segregated and in the intermixed species.

## VI. CONCLUSIONS

Our experimental and theoretical results show that Si and Cr react at room temperature to form an intermixed region  $\sim 10$  monolayers wide. The emission spectra from this region indicate an average Si-rich composition and exhibit a definite metallic character, as shown by the high DOS at  $E_F$  in Figs. 1 and 2. The rapid attenuation of the intrinsic Si surface states at low metal coverages appears related to Si–Cr intermixing.

Room-temperature intermixing at silicon-metal interfaces was previously reported for several Si–near-noble-metal and Si–noble-metal systems.<sup>1,2</sup> The Si–near-noble-metal junctions exhibit metal-rich phases which have an electronic structure close to that of the bulk silicides which nucleate upon moderate heat treatment ( $\text{Ni}_2\text{Si}$ ,  $\text{Pd}_2\text{Si}$ ,  $\text{Pt}_2\text{Si}$ ). For Pd–Si there is evidence of epitaxial growth of a  $\text{Pd}_2\text{Si}$ -like structure.<sup>4</sup>

The only Cr silicide previously known to grow on Si upon reaction at  $450^\circ\text{C}$  is  $\text{CrSi}_2$ , a compound with the C-40-type crystal structure with hexagonal symmetry and nine atoms per unit cell.<sup>9</sup> Shinoda *et al.*<sup>33</sup> reported resistivity measurements and a band gap of  $\sim 0.35$  eV for a  $\text{CrSi}_2$  single crystal. The Schottky-barrier height for the Si– $\text{CrSi}_2$  junction has been reported to be  $\Phi_B = 0.67$  eV.<sup>6</sup> In contrast to this, we have shown that the intermixed species formed at room temperature is metallic and we determined  $\Phi_B = 0.79 \pm 0.1$  eV. It seems clear, therefore, that the observed intermixed phase exhibits fundamental differences compared to  $\text{CrSi}_2$  and we have undertaken photoemission studies of both annealed Cr–Si interfaces and bulk  $\text{CrSi}_2$ .<sup>10</sup>

Several years ago Tu suggested<sup>34</sup> that “interfacial reactions” could explain the strikingly different compound growth kinetics observed at Si–refractory-metal interfaces and other Si–metal systems. We are now at a point where the use of spectroscopic techniques can give a microscopic picture of such reactions and concentrated efforts in this direction seem timely.

## ACKNOWLEDGMENTS

We are grateful to G. W. Rubloff, J. G. Clabes, and B. Reihl for disclosing results prior to publica-

tion, to G. Margaritondo and A. R. Williams for comments and discussions, and to L. Braicovich, O. Bisi, and G. Ottaviani for helpful suggestions. This work was supported by the U. S. Army Research Office under Grant No. DAAG29-81-K-0140. The Synchrotron Radiation Center is supported by the National Science Foundation under Grant No. DMR-7721888, and the assistance of its staff is gratefully acknowledged.

## APPENDIX

In Sec. III we examined the experimental attenuation of the Si  $2p$  emission as a function of metal coverage and compared it (Fig. 4) with the ideal result for a sharp, unreacted interface. Here we will examine the effect of different growth mechanisms of the Cr film on the Si  $2p$  emission, always under the assumption that no reaction occurs at the interface. We will show that the experimental results are not consistent with any of these growth mechanisms and that interface reaction must be considered if the observed behavior is to be explained.

A classification scheme for growth of thin films leads to the distinction between three basic growth modes: the Frank–van der Merwe mode [Fig. 8(a)], the Volmer–Weber mode [Fig. 8(b)], and the Stranski–Krastanov mode [Fig. 8(c)].<sup>35</sup> The actual growth mode for a given system will depend on the relative importance of the film surface energy, substrate surface energy, and the internal strain energy of the film.<sup>35</sup> The Frank–van der Merwe mode is actually a “layer by layer” mechanism that, for the coverage range of interest here, can be approximated by the theoretical curve plotted in Fig. 4 (dashed line), where the emission from the substrate is attenuated exponentially with an attenuation length equal to the escape depth  $L$  for a given kinetic energy. Figure 4 shows that for  $1 < \Theta < 9$  the experimental attenuation rate is much slower than expected for a Frank–van der Merwe non-reactive growth mechanism.

Both the Volmer–Weber and the Stranski–Krastanov mechanisms include three-dimensional island growth of the deposited film. In the first case the islands grow directly on the substrate while in the second case they grow on an intermediate continuous layer [see Fig. 8(c)]. We will take into account three-dimensional island growth assuming hemispherical islands of equal radius  $R$  with an average island concentration of  $n_c$  islands/cm<sup>2</sup>. We expect such a model to be an acceptable approximation of the early stages of island

nucleation. With such simplifications we can use the island concentration  $n_c$  as a fitting parameter independent of coverage in a limited coverage range ( $\Theta \leq 10$ ), and the radius  $R$  of the island will be a simple function of the now "nominal" coverage  $\Theta$ :

$$R = \left( \frac{3p_a N \Theta}{2\pi \rho n_c} \right)^{1/3}, \quad (\text{A1})$$

where  $p_a$  is the atomic weight for Cr,  $\rho$  is the Cr density, and  $N \simeq 7.6 \times 10^{14}$  atoms/cm<sup>2</sup> comes from our definition of monolayer coverage. The total sample area covered by the islands will therefore vary as  $[\Theta]^{2/3}$ , and the condition that we are in the early stages of island nucleation can be roughly expressed by imposing the condition that the covered area is smaller than the total sample area, obtaining

$$\Theta \ll \frac{2\rho}{3p_a N} \frac{1}{\sqrt{\pi n_c}}. \quad (\text{A2})$$

The calculation of the attenuation owing to the presence of such islands is elementary, and we obtain

$$\frac{I_{2p}(\Theta)}{I_{2p}(0)} = 1 - n_c \pi R^2 \{ 1 + n_c 2\pi \times [e^{-R/L}(RL + L^2) - L^2] \} \quad (\text{A3})$$

$$\frac{I_{2p}(\Theta)}{I_{2p}(0)} = 1 - \frac{Np_a}{\rho d} (1 - e^{-d/L}) \Theta \quad \text{for } \Theta \leq \frac{\rho d}{Np_a},$$

$$\frac{I_{2p}(\Theta)}{I_{2p}(0)} = e^{-d/L} (1 - n_c \pi R^2 \{ 1 + n_c 2\pi [e^{-R/L}(RL + L^2) - L^2] \}) \quad \text{for } \Theta \geq \frac{\rho d}{Np_a}. \quad (\text{A6})$$

Equation (A6) simply represents a type (A3) growth following an initial-type (A5) stage.

In Figs. 8(d) and 8(e) we have plotted (solid line) the experimental spectra for the Si 2*p* intensity in the initial stage of the growth, obtained for  $h\nu = 135$  eV photons [Fig. 8(d)] and  $h\nu = 120$  eV photons [Fig. 8(e)]. The dotted line represents plots of the Si 2*p* attenuation during the initial stage (A5) of the Stranski-Krastanov growth for different values of the parameter  $d$ . The dashed lines represent plots of the Si 2*p* intensity during a Volmer-Weber growth (A3).

A comparison of the experimental spectra for  $h\nu = 120$  and  $h\nu = 135$  eV shows the same qualitative coverage dependence of the Si 2*p* emission.

where  $L$  is the photoelectron escape depth at the given energy. Equation (A3) combined with (A1) gives directly the result for a Volmer-Weber growth mechanism.

For the Stranski-Krastanov mode, one has to consider a first stage in which a continuous film of thickness  $d$  (fitting parameter) is formed. For further metal deposition an expression of the type (A3) will hold. We will approximate the first stage by assuming a lateral growth of metal islands of constant thickness  $d$ . The islands will coalesce forming a continuous film for

$$\Theta = \frac{\rho d}{Np_a}. \quad (\text{A4})$$

We can now derive a very simple expression for the Si 2*p* attenuation,

$$\frac{I_{2p}(\Theta)}{I_{2p}(0)} = 1 - \frac{Np_a}{\rho d} (1 - e^{-d/L}) \Theta. \quad (\text{A5})$$

For a Stranski-Krastanov growth mechanism we therefore expect the Si 2*p* attenuation to be linear with coverage in the first growth stage. For the whole growth sequence we will have

An initial region extends up to 1.5–1.75 monolayer followed by a region in which the attenuation rate is faster and the dependence on coverage is roughly linear. Figure 8(d) shows clearly that the first stage of a Stranski-Krastanov growth is not a reasonable approximation for the observed behavior. It is instead possible to find a reasonable choice of the growth parameter that gives some agreement between the experiment and a Volmer-Weber picture [dashed line, number 2 in Fig. 8(d)]. However, the same choice of parameters gives a theoretical curve for  $h\nu = 120$  eV [dashed line, number 2 in Fig. 8(e)] in sharp disagreement with the experimental spectrum. For a Volmer-Weber growth mechanism it is actually impossible to find

one set of parameters that gives reasonable agreement between theory and experiment for both  $h\nu=120$  and  $135$  eV. In Fig. 8(d) the best agreement is obtained for a concentration  $n_c$  of  $1.17 \times 10^{12}$  islands/cm<sup>2</sup>, with an island radius of  $\sim 22$  Å at  $\Theta=3$ , while in Fig. 8(e) we obtained some agreement choosing  $n_c=4.10 \times 10^{10}$  islands/cm<sup>2</sup>, with islands of  $\sim 68$ -Å radius at  $\Theta=3$ . The fact is that in assuming a Volmer-

Weber growth of an unreacted Cr film, the escape depth difference ( $L=5-7$  Å for  $h\nu=135$  eV and  $L=10-12$  Å for  $h\nu=120$  eV) is not enough to explain the strong difference in the attenuation rate of the experimental spectra in Figs. 8(d) and 8(e). Such a difference can be accounted for by assuming that reaction does occur at the interface and that an extended intermixed region forms upon Cr deposition on the Si surface.

- <sup>1</sup>J. N. Miller, S. A. Schwarz, I. Lindau, W. E. Spicer, B. De Michelis, I. Abbati, and L. Braicovich, *J. Vac. Sci. Technol.* **17**, 920 (1980); I. Abbati, L. Braicovich, B. De Michelis, O. Bisi, and R. Rovetta, *Solid State Commun.* **37**, 119 (1981).
- <sup>2</sup>L. Braicovich, I. Abbati, J. N. Miller, I. Lindau, S. Schwarz, P. R. Skeath, C. Y. Su, and W. E. Spicer, *J. Vac. Sci. Technol.* **17**, 1005 (1980); L. Braicovich, C. M. Garner, P. R. Skeath, C. Y. Su, P. W. Chye, I. Lindau, and W. E. Spicer, *Phys. Rev. B* **20**, 5131 (1979).
- <sup>3</sup>C. F. Brucker and L. J. Brillson, *J. Vac. Sci. Technol.* **19**, 617 (1981); *Appl. Phys. Lett.* (in press).
- <sup>4</sup>P. S. Ho, T. Y. Tan, J. E. Lewis, and G. W. Rubloff, *J. Vac. Sci. Technol.* **16**, 1120 (1979); J. L. Freeouf, G. W. Rubloff, P. S. Ho, and T. S. Kuan, *Phys. Rev. Lett.* **43**, 1836 (1979); P. E. Schmid, P. S. Ho, H. Föll, and G. W. Rubloff, *ibid.* **18**, 937 (1981).
- <sup>5</sup>N. W. Cheung, P. J. Grunthaner, F. J. Grunthaner, J. W. Mayer, and B. M. Ullrich, *J. Vac. Sci. Technol.* **18**, 917 (1981); P. J. Grunthaner, F. J. Grunthaner, and J. W. Mayer, *ibid.* **17**, 924 (1980).
- <sup>6</sup>J. M. Andrews and J. C. Phillips, *Phys. Rev. Lett.* **35**, 56 (1975); S. Y. Louie, J. R. Chelikowsky, and M. L. Cohen, *J. Vac. Sci. Technol.* **13**, 790 (1976).
- <sup>7</sup>L. J. Brillson, G. Margaritondo, and N. G. Stoffel, *Phys. Rev. Lett.* **44**, 667 (1980).
- <sup>8</sup>G. Ottaviani, *J. Vac. Sci. Technol.* **16**, 1112 (1979); **18**, 924 (1981); S. P. Murarka, *ibid.* **17**, 775 (1980).
- <sup>9</sup>K. N. Tu, in *Thin Film Interdiffusion and Reactions*, edited by J. M. Poate, K. N. Tu, and J. W. Mayer (Wiley, Chichester, England, 1978).
- <sup>10</sup>J. H. Weaver, V. L. Moruzzi, and F. A. Schmidt, *Phys. Rev. B* **23**, 2916 (1981) for bulk VSi<sub>2</sub>, TaSi<sub>2</sub>, and MoSi<sub>2</sub>; A. Franciosi, J. H. Weaver, D. G. O'Neill, F. A. Schmidt, O. D. McMasters, O. Bisi, and C. Calandra (unpublished) for bulk CrSi<sub>2</sub> and high-temperature interface reaction.
- <sup>11</sup>Selected results for coverages  $\Theta > 1$  were discussed in an earlier paper: A. Franciosi, D. J. Peterman, and J. H. Weaver, *J. Vac. Sci. Technol.* **19**, 657 (1981).
- <sup>12</sup>G. Margaritondo, J. H. Weaver, and N. G. Stoffel, *J. Phys. E* **12**, 662 (1979).
- <sup>13</sup>Such stringent operating conditions were imposed by the high reactivity of the refractory metals; in those instances where the pressure rose to  $6-7 \times 10^{-10}$  Torr during evaporation, contamination of the evaporated metal film and modification of the interface behavior was observed.
- <sup>14</sup>The ASW method as developed by A. R. Williams, J. Kübler, and C. D. Gelatt [*Phys. Rev. B* **19**, 6094 (1979)] is the spherical wave analog of Slater's augmented-plane-wave (APW) method and is closely related to Andersen's linear combination of muffin tin orbitals (LMTO) method (see Ref. 15).
- <sup>15</sup>O. K. Andersen, *Phys. Rev. B* **12**, 3060 (1975).
- <sup>16</sup>L. F. Wagner and W. E. Spicer, *Phys. Rev. Lett.* **28**, 1381 (1972); J. E. Rowe, M. M. Traum, and N. V. Smith, *ibid.* **33**, 1333 (1974).
- <sup>17</sup>J. Barth, F. Gerken, K. L. I. Kobayashi, J. H. Weaver, and B. Sonntag, *J. Phys. C* **13**, 1369 (1980), and our own unpublished results for thick layers of Cr deposited onto oxidized Ta substrates. All of the results discussed for thick films agree with what we found for cleaved bulk samples of Cr.
- <sup>18</sup>I. Lindau and W. E. Spicer, *J. Electron. Spectros. Relat. Phenom.* **3**, 409 (1974).
- <sup>19</sup>First-principles calculation of a silicide electronic structure is usually a difficult and expensive task due to the large number of atoms per unit cell and to the complicated crystal structure which determines the set of basis function to use. CrSi<sub>2</sub>, for example, exhibits the C-40 structure with hexagonal symmetry and nine atoms per unit cell. Hence, theoretical information is often obtained with semiempirical approaches or with calculations for simplified lattice structures, as in this paper.
- <sup>20</sup>Similar calculations were performed (see Ref. 10) for a number of refractory metal silicides and the systematic trends allowed the interpretation of photoemission spectra of bulk VSi<sub>2</sub>, TaSi<sub>2</sub>, and MoSi<sub>2</sub>.
- <sup>21</sup>P. S. Ho, G. W. Rubloff, J. E. Lewis, V. L. Moruzzi, and A. R. Williams, *Phys. Rev. B* **22**, 4784 (1980).
- <sup>22</sup>O. Bisi and C. Calandra, *J. Phys. C* **14**, 5479 (1981).
- <sup>23</sup>J. Rath and J. Callaway, *Phys. Rev. B* **8**, 5398 (1973); the more recent calculations by D. G. Laurent, J. Callaway, J. L. Fry, and N. E. Brener, *Phys. Rev. B* **23**, 4977 (1981) gave a virtually identical density of states.

- <sup>24</sup>The number of electrons per atom that correspond to a given feature in the DOS can be easily obtained remembering that the structures  $\text{Cu}_3\text{Au}$ ,  $\text{CuAu}$ , and  $\text{CuAu}_3$  have just one formula unit per cell.
- <sup>25</sup>In the present case the only available Cr core level was the shallow  $3p$  with overall photoemission intensity that made it unsuitable for coverage-dependent studies. Even in those cases where it is possible to monitor core binding energy shifts of both elements upon binary compound formation, the observed "chemical shift" need not be related in an elementary way to the actual charge transfer; see, for instance, R. E. Watson and M. L. Perlman, *Struct. Bonding* **24**, 82 (1975). Charge transfer in energy band calculations is difficult to define because it depends on the manner in which space is allocated to the different constituents. As a further complication, we vary the lattice constant of the compound (by systematically changing the sphere volumes of the constituents) in order to determine the minimum total energy (theoretical equilibrium). In our calculations, the space allocation of the constituents is determined by calculated bulk moduli and volumes of the constituents in their elemental forms. In changing the volume of the compound (to find theoretical equilibrium), a constituent with a large elemental volume and a small elemental bulk modulus suffers a larger volume change than one with a small elemental volume and a large elemental bulk modulus. The charge transfers referred to in this work are all based on this construction.
- <sup>26</sup>D. E. Eastman, F. J. Himpsel, J. A. Knapp, and K. C. Pandey, in *Proceedings of the 14th International Semiconductor Conference, Edinburgh, 1978*, edited by B. L. H. Wilson (Institute of Physics and Physical Society, London, 1979).
- <sup>27</sup>D. E. Eastman, *Phys. Rev. B* **2**, 1 (1970); H. B. Michaelson, *J. Appl. Phys.* **48**, 4279 (1977).
- <sup>28</sup>F. G. Allen and G. W. Gobeli, *J. Appl. Phys.* **35**, 597 (1964); M. Erbudak and T. E. Fischer, *Phys. Rev. Lett.* **29**, 732 (1972); J. E. Rowe, *Phys. Lett.* **46A**, 400 (1974); J. E. Rowe, H. Ibach, and H. Froitzheim, *Surf. Sci.* **48**, 44 (1975); W. Mönch, *ibid.* **63**, 79 (1977).
- <sup>29</sup>P. S. Ho, P. E. Schmid, and H. Föll, *Phys. Rev. Lett.* **46**, 782 (1981); G. W. Rubloff, P. S. Ho, J. L. Freeouf, and J. E. Lewis, *Phys. Rev. B* **23**, 4183 (1981).
- <sup>30</sup>G. V. Hansson, R. Z. Bachrach, R. S. Bauer, and P. Chiaradia, *Phys. Rev. Lett.* **46**, 1033 (1981); *J. Vac. Sci. Technol.* **18**, 559 (1981).
- <sup>31</sup>I. Abbati, G. Rossi, I. Lindau, and W. E. Spicer, *J. Vac. Sci. Technol.* **19**, 636 (1981); G. Rossi, I. Abbati, L. Braicovich, I. Lindau, and W. E. Spicer, *Solid State Commun.* **39**, 195 (1981).
- <sup>32</sup>J. G. Clabes and G. W. Rubloff, *J. Vac. Sci. Technol.* **18**, 903 (1981); J. G. Clabes (private communication).
- <sup>33</sup>D. Shinoda, S. Asanabe, and Y. Sasaki, *J. Phys. Soc. Jpn.* **19**, 269 (1964).
- <sup>34</sup>K. N. Tu, *Appl. Phys. Lett.* **27**, 221 (1975); R. W. Bower and J. W. Mayer, *ibid.* **20**, 359 (1972).
- <sup>35</sup>E. Bauer and H. Poppa, *Thin Solid Films* **12**, 167 (1972), and references therein.